

The effective slip-length tensor for a flow over weakly slipping stripes

Evgeny S. Asmolov,^{1,2,3} Jiajia Zhou,⁴ Friederike Schmid,⁴ and
Olga I. Vinogradova^{1,5,6}

¹A.N. Frumkin Institute of Physical Chemistry and Electrochemistry, Russian Academy of Sciences, 31 Leninsky Prospect, 119991 Moscow, Russia

²Central Aero-Hydrodynamic Institute, 140180 Zhukovsky, Moscow region, Russia

³Institute of Mechanics, M. V. Lomonosov Moscow State University, 119991 Moscow, Russia

⁴Institut für Physik, Johannes Gutenberg-Universität Mainz, 55099 Mainz, Germany

⁵Department of Physics, M. V. Lomonosov Moscow State University, 119991 Moscow, Russia

⁶DWI, RWTH Aachen, Forckenbeckstr. 50, 52056 Aachen, Germany

(Received 27 December 2012)

We discuss the flow past a flat heterogeneous solid surface decorated by slipping stripes. The spatially varying slip length, $b(y)$, is assumed to be small compared to the scale of the heterogeneities, but finite. For such weakly slipping surfaces, earlier analyses have predicted that the effective slip length is simply given by the surface-averaged slip length, which implies that the effective slip-length tensor becomes isotropic. Here we show that a different scenario is expected if the local slip length has step-like jumps at the edges of slipping heterogeneities. In this case, the next-to-leading term in an expansion of the effective slip-length tensor in powers of $\max(b(y))$ becomes comparable to the leading-order term, but anisotropic, even at very small $b(y)$. This leads to an anisotropy of the effective slip even for very weakly slipping stripes, and to a significant reduction compared to the surface-averaged value. The asymptotic formulae are tested by numerical solutions and dissipative particle dynamics simulations.

1. Introduction

With emerging technologies in microfluidics (Stone *et al.* 2004; Squires & Quake 2005), there has been renewed interest in quantifying the effects of surface chemical heterogeneities with local scalar slip (Vinogradova 1999; Lauga *et al.* 2007) on fluid motion. Well-known examples of such heterogeneous systems include composite superhydrophobic (Cassie) surfaces, where a gas layer is stabilized by a rough wall texture (Quere 2008). For these surfaces effective slip lengths are often very large compared with the value on flat solids (Bocquet & Barrat 2007; Vinogradova & Belyaev 2011), so that they have the potential to influence microfluidics (or to extend microfluidic systems to nanofluidics), by generating very fast and well-controlled flows in small devices (Vinogradova & Dubov 2012).

In such situations it is convenient to construct so-called effective slip boundary conditions, where the complex flow pattern at a heterogeneous surface is replaced by an effective flow averaged over the length scale of the experimental configuration (Vinogradova & Belyaev 2011; Kamrin *et al.* 2010). In other words, rather than trying to solve equations of motion on the scale of the individual corrugation or pattern, one considers the macroscale fluid motion (on the scale larger than the pattern characteristic length) by using macroscopically equivalent boundary conditions for an imaginary smooth surface. Such an effective

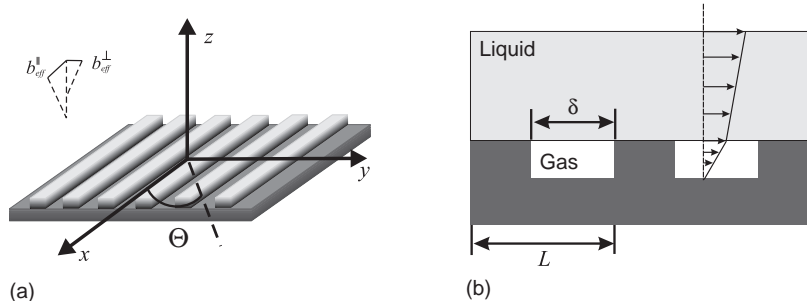


FIGURE 1. Sketch of the striped surface: $\Theta = \pi/2$ corresponds to transverse stripes, $\Theta = 0$ to longitudinal stripes.

condition mimics the actual one along the true heterogeneous surface. It fully characterizes the flow at the real surface and can be used to solve complex hydrodynamic problems with much reduced computational effort. The effective slip approach has been supported by statistical diffusion arguments (Bazant & Vinogradova 2008), justified for the case of Stokes flow over a broad class of surfaces (Kamrin *et al.* 2010), and recently confirmed by computer simulations (Priezjev 2011; Schmieschek *et al.* 2012; Zhou *et al.* 2012).

For an anisotropic texture, the effective boundary condition generally depends on the direction of the flow and is a tensor, $\mathbf{b}_{\text{eff}} \equiv \{b_{ij}^{\text{eff}}\}$, represented by a symmetric, positive definite 2×2 matrix, which can be diagonalized by a rotation with angle Θ (Figure 1). For all anisotropic surfaces its eigenvalues $b_{\text{eff}}^{\parallel}$ and b_{eff}^{\perp} correspond to the fastest (greatest forward slip) and slowest (least forward slip) orthogonal directions (Bazant & Vinogradova 2008). In the general case of arbitrary direction Θ , the flow past such surfaces with anisotropic effective slip becomes misaligned with the driving force. Therefore, anisotropic textures can potentially be used to generate transverse hydrodynamic flow (Ajdari 2002; Bazant & Vinogradova 2008; Stroock *et al.* 2002a), which is of obvious fundamental and practical interest. For example, transverse hydrodynamic couplings in flow through a textured channel can be used to separate/concentrate suspended particles (Gao & Gilchrist 2008) or for passive chaotic mixing (Stroock *et al.* 2002a,b). This can also be used to generate anisotropic electrokinetic flows (Bahga *et al.* 2010; Belyaev & Vinogradova 2011; Squires 2008).

However, it has been predicted that regardless of the anisotropy of the surface texture, the effective slip-length tensor, \mathbf{b}_{eff} , becomes isotropic ($b_{\text{eff}}^{\perp} = b_{\text{eff}}^{\parallel}$) for a *weakly* slipping pattern, i.e. when the local slip length, b , is small compared to the characteristic scale of heterogeneities, L . The value of the effective slip is the surface average of the local slip length, $\mathbf{b}_{\text{eff}} = \mathbf{I} \langle b(x, y) \rangle$. In the particular case of a no-slip plane covered by patterns with constant slip length b – the situation considered in most previous publications on the subject (Priezjev *et al.* 2005; Ybert *et al.* 2007; Feuillebois *et al.* 2009) – one can easily derive (Belyaev & Vinogradova 2010a; Kamrin *et al.* 2010)

$$b_{\text{eff}}^{\parallel, \perp} \simeq b\phi, \quad (1.1)$$

where $\phi = \delta/L$ is the surface fraction of the slipping phase. This result implies, among other, that the flow aligns with the applied driving force for all in-plane directions. Thus, it seems impossible to generate transverse hydrodynamic (Vinogradova & Belyaev 2011; Zhou *et al.* 2012) or transverse electro-osmotic (Belyaev & Vinogradova 2011) phenomena for weakly slipping anisotropic textures. Another important, and somewhat remark-

able, consequence of Eq. (1.1) is that the effective slip is predicted to depend only on the fractions of slipping areas, but not on their detailed structure. Known derivations of Eq. (1.1), however, neglect localized flow perturbations around possible jumps in discrete slip lengths, from 0 to b , at the border of heterogeneities.

In the present paper we reconsider this problem, focussing on the situation where the perturbation $b(x, y)$ is piecewise constant, i.e., it jumps in a step-like fashion at heterogeneity boundaries. In Sec. 2 we define the problem and prove that known two-term expansions for effective slip lengths of one-dimensional textures (Kamrin *et al.* 2010) are not valid for discontinuous local slip. Then in Sec. 3 we construct the expansions for the eigenvalues of the slip-length tensor of alternating weakly slipping stripes. Here we also analyze a singularity of the velocity gradient at the edges of stripes. The details of the computer simulation method (dissipative particle dynamics) are discussed in Sec. 4. Finally, in Sec. 5, we present simulation and numerical results to validate the predictions of the asymptotic theory. The practical implications and limitations of our models are also reviewed here. A brief description of the numerical scheme is given in Appendix A.

2. Problem set-up

We consider a creeping flow along a planar anisotropic wall, and a Cartesian coordinate system (x, y, z) (Figure 1). The origin of coordinates is placed at the flat interface, a 1D texture varies over a period L . Our analysis is based on the limit of a thick channel or a single interface, so that the velocity profile sufficiently far above the surface may be considered as a linear shear flow. Dimensionless variables are defined in terms of the reference length scale L , the asymptotic shear rate far above the surface, G , and the fluid kinematic viscosity, ν .

For a one-dimensional texture there exists a simple relation between longitudinal and transverse effective slip lengths (Asmolov & Vinogradova 2012)

$$b_{\text{eff}}^{\perp}[b(y)] = \frac{b_{\text{eff}}^{\parallel}[2b(y)]}{2}. \quad (2.1)$$

Therefore, it is sufficient to consider the longitudinal configuration. Since in this case, the velocity has only one component, we seek a solution for the velocity profile of the form

$$v = U + u,$$

where $U = z$ is the undisturbed linear shear flow. The perturbation of the flow $u(y, z)$, which is caused by the presence of the texture and decays far from the surface at small Reynolds number $Re = GL^2/\nu$, satisfies the dimensionless Laplace equation,

$$\Delta u = 0. \quad (2.2)$$

The boundary conditions at the wall and at infinity are defined as

$$z = 0 : \quad u - \varepsilon\beta(y) \partial_z u = \varepsilon\beta(y), \quad (2.3)$$

$$z \rightarrow \infty : \quad \partial_z u = 0, \quad (2.4)$$

where $\varepsilon = b_{\text{max}}/L$ and $\beta = b(y)/b_{\text{max}}$ is the normalized slip length.

For a weakly slipping anisotropic texture, $\varepsilon \ll 1$, an expansion in powers of ε yields to leading order an area-averaged isotropic slip length (Belyaev & Vinogradova 2010a). In practice, this means that the slip-length tensor becomes isotropic and that for all in-plane directions, the flow aligns with the applied force. A similar conclusion has been reached by Kamrin *et al.* (2010). The authors constructed an asymptotic series for 3D

flow \mathbf{u} over an arbitrary weakly slipping 2D texture with a locally varying slip length $\beta(x, y)$:

$$\mathbf{u} = \sum_{k=1}^{\infty} \varepsilon^k \mathbf{u}_k^{KBS}. \quad (2.5)$$

For 1D textures, the boundary conditions to u_k^{KBS} can be readily obtained by substituting Eq. (2.5) into Eq. (2.3) and by collecting the terms of the order of ε^k :

$$\begin{aligned} z = 0 : \quad & u_1^{KBS} = \beta(x, y), \\ k > 1 : \quad & u_k^{KBS} = \beta(x, y) \partial_z u_{k-1}^{KBS}. \end{aligned} \quad (2.6)$$

If we consider periodic textures with $\beta(y)$ being an even function, the slip length can be expanded as a cosine Fourier series:

$$\beta = \frac{\tilde{\beta}^0}{2} + \sum_{n=1}^{\infty} \tilde{\beta}^n \cos(2\pi n y), \quad (2.7)$$

$$\tilde{\beta}^n = 2 \int_{-1/2}^{1/2} \beta(y) \cos(2\pi n y) dy. \quad (2.8)$$

The expansions of the effective slip lengths for 1D textures up to second order in ε of the effective slip lengths are then given by (Kamrin *et al.* 2010)

$$b_{\text{eff}}^{\parallel}/L = \varepsilon \frac{\tilde{\beta}^0}{2} - \varepsilon^2 \pi \sum_{n=1}^{\infty} n |\tilde{\beta}^n|^2, \quad (2.9)$$

$$b_{\text{eff}}^{\perp}/L = \varepsilon \frac{\tilde{\beta}^0}{2} - \varepsilon^2 2\pi \sum_{n=1}^{\infty} n |\tilde{\beta}^n|^2. \quad (2.10)$$

The first-order terms are the isotropic part of the effective slip, Eq. (1.1). The second-order terms, which can be neglected for a weakly slipping patterns, are expected to introduce the influence of the surface structure, and are responsible for the anisotropy of the flow.

The argument presented above implicitly assumes that the infinite sums over n in the higher-order expansion coefficients converge, which implies that the Fourier series, Eq. (2.7), can be differentiated infinitely often with respect to y . In cases of discontinuous slip, where $\beta(y)$ exhibits jumps, this is no longer correct and the argument breaks down. From a physical point of view, the problem can be associated with singularities of the velocity gradient at the boundaries of the slip region. As a specific example, let us consider a classical case of alternating weakly slipping ($\varepsilon = b_0/L \ll 1$) stripes with

$$\beta(y) = \begin{cases} 1 & \text{as } |y| \leq \phi/2 \\ 0 & \text{as } \phi/2 < |y| \leq 1/2 \end{cases}, \quad (2.11)$$

so that the boundary conditions, Eq. (2.3), can be rewritten as

$$\begin{aligned} z = 0, |y| \leq \phi/2 : \quad & u - \varepsilon \partial_z u = \varepsilon, \\ \phi/2 < |y| < 1/2 : \quad & u = 0. \end{aligned} \quad (2.12)$$

The Fourier coefficients for this texture then follow from Eq. (2.8)

$$\begin{aligned} \tilde{\beta}^0 &= 2\phi, \\ n > 0 : \quad \tilde{\beta}^n &= \frac{2 \sin(\pi n \phi)}{\pi n}. \end{aligned} \quad (2.13)$$

This implies that series in Eqs. (2.9) and (2.10),

$$\sum_{n=1}^{\infty} n \left| \tilde{\beta}^n \right|^2 = \frac{2}{\pi^2} \sum_{n=1}^{\infty} \frac{1 - \cos(2\pi n\phi)}{n}, \quad (2.14)$$

diverge, since their terms decay as n^{-1} at $n \rightarrow \infty$ (large n correspond to small length scales). The slow decay of $\left| \tilde{\beta}^n \right|^2$ with n and the divergence of the series indicate that the expansion (2.5) does not resolve properly the solution at small length scales. The velocity gradient grows infinitely near the edge of the slip region (see Sec. 3.2 for a detailed analysis). As a result, the corresponding term in Eq. (2.12), $\varepsilon \partial_z u$, has the same order of magnitude as u in the vicinity of the slipping boundary. Therefore, it cannot be neglected compared to the leading order, even though ε is small.

3. Weakly slipping stripes

3.1. Slip-length tensor.

We now consider the case of stripes more specifically. We first compute the eigenvalues of the effective slip-length tensor. Since we assume only weak local slippage, we evaluate the effective slip length in the principal directions to second order in ε and seek for a solution which is finite, i.e., has no singularity.

A general solution satisfying the Laplace equation (2.2) and decaying at infinity can be presented in terms of a cosine Fourier series as (Asmolov & Vinogradova 2012)

$$u = \frac{a^0}{2} + \sum_{n=1}^{\infty} a^n \exp(-2\pi n z) \cos(2\pi n y), \quad (3.1)$$

where a^n are constant coefficients to be found from (2.12). We construct the asymptotic series for alternating stripes,

$$u = \sum_{k=1}^{\infty} u_k, \quad a^n = \sum_{k=1}^{\infty} a_k^n,$$

imposing that $|u_{k+1}/u_k| \ll 1$ over the entire flow region. The boundary conditions for u_k at the wall can be chosen as follows:

$$z = 0 : \quad u_k - \varepsilon \partial_z u_k = r_k(y), \quad (3.2)$$

$$r_1 = \begin{cases} \varepsilon & \text{as } |y| \leq \phi/2 \\ 0 & \text{as } \phi/2 < |y| \leq 1/2 \end{cases}, \quad (3.3)$$

$$k > 1 : \quad r_k = \begin{cases} 0 & \text{as } |y| \leq \phi/2 \\ -\varepsilon \partial_z u_{k-1} & \text{as } \phi/2 < |y| \leq 1/2 \end{cases}. \quad (3.4)$$

The reader may check by the summation of Eqs. (3.2) over k that they are fully equivalent to Eq. (2.12).

The slip velocity is then

$$u_{slip} = \sum_{k=1}^{\infty} a_k^0/2.$$

The boundary condition (3.2) can be rewritten in terms of Fourier coefficients as

$$\frac{a_k^0}{2} + \sum_{n=1}^{\infty} a_k^n (1 + 2\pi \varepsilon n) \cos(2\pi n y) = r_k(y).$$

The coefficients a_k^n are now determined using the inverse Fourier transform:

$$\begin{aligned} a_k^0 &= 2 \int_{-1/2}^{1/2} r_k(y) dy, \\ n > 0 : \quad a_k^n &= \frac{2}{1 + 2\pi\epsilon n} \int_{-1/2}^{1/2} r_k(y) \cos(2\pi n y) dy. \end{aligned} \quad (3.5)$$

From Eqs. (3.3) and (3.5), we have to leading order in ϵ

$$\begin{aligned} a_1^0 &= 2\epsilon\phi, \\ n > 0 : \quad a_1^n &= \frac{2\epsilon \sin(\pi n \phi)}{\pi n (1 + 2\pi\epsilon n)}. \end{aligned}$$

To find the second-order terms we must evaluate $r_2 = \partial_z u_1$, which gives

$$\partial_z u_1 = - \sum_{n=1}^{\infty} a_1^n 2\pi n \cos(2\pi n y) = -4\epsilon \sum_{n=1}^{\infty} \frac{\sin(\pi n \phi) \cos(2\pi n y)}{1 + 2\pi\epsilon n}. \quad (3.6)$$

The second-order slip velocity is then

$$a_2^0 = -4 \int_{\phi/2}^{1/2} \epsilon \partial_z u_1 dy = -\frac{8\epsilon^2}{\pi} \sum_{n=1}^{\infty} \frac{\sin^2(\pi n \phi)}{n(1 + 2\pi\epsilon n)} \quad (3.7)$$

$$= -\frac{4\epsilon^2}{\pi} \left[\sum_{n=1}^{\infty} \frac{1}{n(1 + 2\pi\epsilon n)} - \sum_{n=1}^{\infty} \frac{\cos(2\pi n \phi)}{n} + O(\epsilon) \right] \quad (3.8)$$

$$= \frac{4\epsilon^2}{\pi} \left\{ \ln(2\pi\epsilon) - \gamma - \frac{1}{2} \ln[4 \sin^2(\pi \phi)] \right\} + O(\epsilon^3), \quad (3.9)$$

where $\gamma = 0.5772157\dots$ is Euler's constant. The series in (3.8) are very similar to those in (2.14). They differ only by the factor $(1 + 2\pi\epsilon n)$ in the denominator of the first sum. This factor is small at $n \sim 1$, but it grows linearly with n at large n , thus ensuring convergence of the series. Note that the first logarithmic term in (3.9) does not depend on the fraction of the slip regions, ϕ . This term is associated with the flow singularities near the boundaries between no-slip and slip regions (see Subsection 3.2), which are responsible for additional viscous dissipation that reduces b_{eff} .

Finally, for the longitudinal effective slip we obtain the following expansion

$$b_{\text{eff}}^{\parallel}/L = \epsilon\phi + \frac{2\epsilon^2}{\pi} \left\{ \ln \left[\frac{\pi\epsilon}{\sin(\pi\phi)} \right] - \gamma \right\} + O(\epsilon^3 \ln \epsilon), \quad (3.10)$$

from which we can derive the transverse effective slip using (2.1),

$$b_{\text{eff}}^{\perp}/L = \epsilon\phi + \frac{4\epsilon^2}{\pi} \left\{ \ln \left[\frac{2\pi\epsilon}{\sin(\pi\phi)} \right] - \gamma \right\} + O(\epsilon^3 \ln \epsilon). \quad (3.11)$$

To summarize, we have here directly demonstrated that Eq. (1.1) must be applied with care. On the one hand, Eqs. (3.10) and (3.11) unambiguously show that Eq. (1.1) does indeed give the correct first-order term of an expansion for the eigenvalues of the slip-length tensor, even in a case of alternating stripes. On the other hand, the higher order contributions may be nonanalytical in ϵ , which may create complications. In case of a local slip which exhibits step-like jumps at the edge of heterogeneities, the second-order terms of the expansions become of the order of $\epsilon^2 \ln \epsilon$ (in contrast to ϵ^2 , which would be expected for continuously varying local slip). Therefore, they can be comparable to the

first-order terms and cannot be ignored even at relatively small ε (see Section 5). These terms are not only responsible for anisotropy of the flow, but also (being negative) for an additional dissipation.

3.2. Edge singularity

We now describe the flow singularities near slipping heterogeneities in more detail. Wang (2003) has considered the flow over a surface with rectangular grooves, and found that the shear stress is singular near sharp corners, i.e., proportional to $r^{-1/3}$ for longitudinal and to $r^{-0.455}$, for transverse configurations. Here r is the distance from the corner. Following this approach, we now consider the flow in the vicinity of the edge of our weakly slipping regions, by using polar coordinates (r, θ) with the origin in $(y, z) = (\phi/2, 0)$. The no-slip and slip regions then correspond to $\theta = 0$ and $\theta = \pi$. The solution of the Laplace equation (2.2) that satisfies the no-slip boundary condition at $\theta = 0$ is

$$u = cr^\lambda \sin(\lambda\theta). \quad (3.12)$$

The velocity at the edge is finite provided $\lambda > 0$. The components of velocity gradient are

$$\partial_z u = c\lambda r^{\lambda-1} \cos[\theta(1-\lambda)], \quad \partial_y u = -c\lambda r^{\lambda-1} \sin[\theta(1-\lambda)]. \quad (3.13)$$

The velocity decays faster than its gradient as $r \rightarrow 0$: r^λ vs. $r^{\lambda-1}$. Hence, in a small region $r \sim \varepsilon$, the dimensionless shear rate $\varepsilon \partial_z u$ is of the same order as u , and cannot be ignored in the boundary condition (2.12) even though $\varepsilon \ll 1$. Moreover, at smaller distances, $r \ll \varepsilon$, the term $\varepsilon \partial_z u$ dominates over u , and the condition in this region becomes shear-free:

$$r \ll \varepsilon, \theta = \pi: \quad \partial_z u = 0. \quad (3.14)$$

The last condition enables us to find λ . To satisfy Eq. (3.14) one should require, in view of (3.13), $\lambda = 1/2$. Therefore, the velocity over the slip region is

$$r \ll \varepsilon, \theta = \pi: \quad u = cr^{1/2}, \quad \partial_y u = -cr^{-1/2}/2, \quad (3.15)$$

where c is a constant. The velocity gradient over the no-slip region follows from (3.13):

$$r \ll \varepsilon, \theta = 0: \quad \partial_z u = cr^{-1/2}/2. \quad (3.16)$$

In other words, the shear stress has a singularity at the edge.

We remark that Eqs. (3.15) and (3.16) are valid in a small region, $r \ll b/L$, $r \ll 1$, near a jump in the discrete local slip length, from 0 to a finite b . Therefore, our asymptotic theory is only valid provided that the fractions of the slip and no-slip regions are not too small, $\phi \gg \varepsilon$, $1 - \phi \gg \varepsilon$. Otherwise, the two edges of heterogeneities are close to each other, so that the singular regions overlap. Note that a similar, $r^{-1/2}$, dependence of the velocity has been obtained earlier for a no-slip surface decorated with perfect-slip stripes (Sbragaglia & Prosperetti 2007; Asmolov & Vinogradova 2012).

For the transverse flow one can use the relation between the velocity fields for the two orientations (Asmolov & Vinogradova 2012):

$$v = \frac{1}{2} \left(u_d + z \frac{\partial u_d}{\partial z} \right), \quad w = -\frac{z}{2} \frac{\partial u_d}{\partial y}, \quad (3.17)$$

$$p = -\frac{\partial u_d}{\partial y}, \quad (3.18)$$

where $u_d(y, z) = u[y, z, 2\varepsilon\beta(y)]$ is the velocity field for the longitudinal pattern with

double local slip length (cf. Eq. (2.1). Hence we conclude that at the wall

$$z = 0 : \quad v = \frac{1}{2}u_d, \quad \frac{\partial v}{\partial z} = \frac{\partial u_d}{\partial z}. \quad (3.19)$$

From Eqs. (3.15) - (3.18), it also follows that $\frac{\partial v}{\partial z}$, $\frac{\partial w}{\partial z}$ and p all have the same singularity $r^{-1/2}$ at the edge of weakly slipping region.

4. Simulation method

Our simulations are performed using Dissipative Particle Dynamics (Koelman & Hoogerbrugge 1993; Español & Warren 1995; Groot & Warren 1997), an established method for mesoscale fluid simulations. The DPD method is a coarse-grained, momentum-conserving simulation technique, which naturally includes thermal fluctuations. More specifically, we use a DPD version without conservative interactions (Soddemann *et al.* 2003) and combine that with a tunable-slip method (Smiatek *et al.* 2008) which allows one to implement arbitrary hydrodynamic boundary condition.

The basic DPD equations involve pair interaction between fluid particles. The force exerted by particle j on particle i is given by

$$\mathbf{F}_{ij}^{DPD} = \mathbf{F}_{ij}^D + \mathbf{F}_{ij}^R. \quad (4.1)$$

The dissipative part \mathbf{F}_{ij}^D is proportional to the relative velocity between two particles,

$$\mathbf{F}_{ij}^D = -\gamma_{DPD} \omega_D(r_{ij})(\mathbf{v}_{ij} \cdot \hat{\mathbf{r}}_{ij})\hat{\mathbf{r}}_{ij} \quad (4.2)$$

with the friction coefficient γ_{DPD} . The weight function $\omega_D(r_{ij})$ is a monotonically decreasing function of r_{ij} and vanishes at a given cutoff r_c . The random force \mathbf{F}_{ij}^R has the form

$$\mathbf{F}_{ij}^R = \sqrt{2k_B T \gamma_{DPD} \omega_D(r_{ij})} \xi_{ij} \hat{\mathbf{r}}_{ij}, \quad (4.3)$$

where $\xi_{ij} = \xi_{ji}$ are symmetric, but otherwise uncorrelated random functions with zero mean and variance $\langle \xi_{ij}(t) \xi_{ij}(t') \rangle = \delta(t - t')$ (here $\delta(t)$ is Dirac's delta function). The magnitude of the stochastic contribution is related to the dissipative part by the fluctuation-dissipation theorem to ensure correct equilibrium statistics. The pair forces between two particles satisfy Newton's third law, $\mathbf{F}_{ij} = -\mathbf{F}_{ji}$, and hence the momentum is conserved. This leads to correct long-time hydrodynamic behavior (*i.e.* Navier-Stokes).

The wall interaction is introduced in the same spirit. The force on particle i from the channel is given by

$$\mathbf{F}_i^{wall} = \mathbf{F}_i^{WCA} + \mathbf{F}_i^D + \mathbf{F}_i^R. \quad (4.4)$$

The first one is a repulsive interaction to prevent the fluid particles from penetrating the wall. It can be written in terms of the gradient of a Weeks-Chandler-Andersen (WCA) potential

$$\mathbf{F}_i^{WCA} = -\nabla \cdot V(z), \quad V(z) = \begin{cases} 4\epsilon[(\frac{\sigma}{z})^{12} - (\frac{\sigma}{z})^6 + \frac{1}{4}] & z < 2^{1/6}\sigma \\ 0 & z \geq 2^{1/6}\sigma \end{cases} \quad (4.5)$$

where z is the distance between the fluid particle and the wall. The dissipative contribution is similar to Eq. (4.2), with the velocity difference \mathbf{v}_{ij} replaced by the particle velocity relative to the wall,

$$\mathbf{F}_i^D = -\gamma_L \omega_L(z)(\mathbf{v}_i - \mathbf{v}_{wall}). \quad (4.6)$$

The parameter γ_L characterizes the strength of the wall friction and can be used to tune

Fluid density ρ	$3.75\sigma^{-3}$
Friction coefficient for DPD interaction γ_{DPD}	$5.0\sqrt{m\epsilon}/\sigma$
Cutoff for DPD interaction r_c	1.0σ
Coefficient γ_L for no-slip boundaries	$5.26\sqrt{m\epsilon}/\sigma$
Cutoff for wall interaction	2.0σ
Coefficients γ_L for slip boundaries	$\{0.5, 0.4, 0.3, 0.2, 0.1\}\sqrt{m\epsilon}/\sigma$
Corresponding slip lengths b	$\{2.6, 3.4, 4.7, 7.1, 14.5\} \pm 0.1\sigma$
Shear viscosity η_s	$1.35 \pm 0.01\sqrt{m\epsilon}/\sigma^2$
Position of hydrodynamic boundary	$1.06 \pm 0.12\sigma$

TABLE 1. Parameters used in the DPD simulations.

the value of the slip length. For example, $\gamma_L = 0$ corresponds to perfectly slippery wall, while a positive value of γ_L leads to a finite slip length. The random term has the form

$$\mathbf{F}_i^R = \sqrt{2k_B T \gamma_L \omega_L(z)} \boldsymbol{\xi}_i, \quad (4.7)$$

where each component of $\boldsymbol{\xi}_i$ is an independent random variable function with zero mean and variance $\langle \xi_{i,\alpha}(t) \xi_{i,\alpha}(t') \rangle = \delta(t - t')$.

The simulations are carried out using the open source simulation package ESPResSo (Limbach *et al.* 2006). We use a quadratically decaying weight function $\omega_D(r)$ and a linearly decaying weight function $\omega_L(r)$. Table 1 summarizes the simulation parameters. The most important quantity is the slip length b , which can be estimated from the simulation parameters using an analytical formula due to Smiatek *et al.* (2008). However, the accuracy of the analytic prediction is not satisfactory for weakly slipping surfaces. We simulated plane Poiseuille and Couette flows with various γ_L to obtain the slip length and the position of the hydrodynamic boundary (see Smiatek *et al.* (2008) for details). Poiseuille flow was implemented by applying a constant body force of the order $10^{-4}\epsilon/\sigma$ to all particles.

In the simulations, the patterned surface has a stripe spacing of $L = 100\sigma$. The simulation box is a rectangular cuboid of size $20\sigma \times 100\sigma \times 102\sigma$. Periodic boundary conditions are used in the xy plane. The integration time step is $0.01\sqrt{m/\epsilon}\sigma$. Due to the large system size, the time for reaching a steady state is also quite large (over 10^6 time steps). For weakly slipping surfaces, the flow velocity near the wall is small compared to the thermal fluctuations; thus long simulation times are also required to obtain enough statistics. In this work, velocity profiles have been averaged over 2×10^5 time steps.

Based on the values of the velocities close to the surface, we can estimate the characteristic Reynolds number of our system. Typical Reynolds numbers in our simulations are of order 10, which is much larger than typical values in microfluidic devices. Thus, inertia effects may become important in the simulations, and the Stokes equation is not strictly valid. We shall see below that this slightly affects our simulation results. To reach more realistic Reynolds numbers, one would have to reduce the shear rate by four orders of magnitude. This would reduce the average flow velocity significantly, and the necessary simulation time to gather data with sufficiently good statistics will then increase prohibitively.

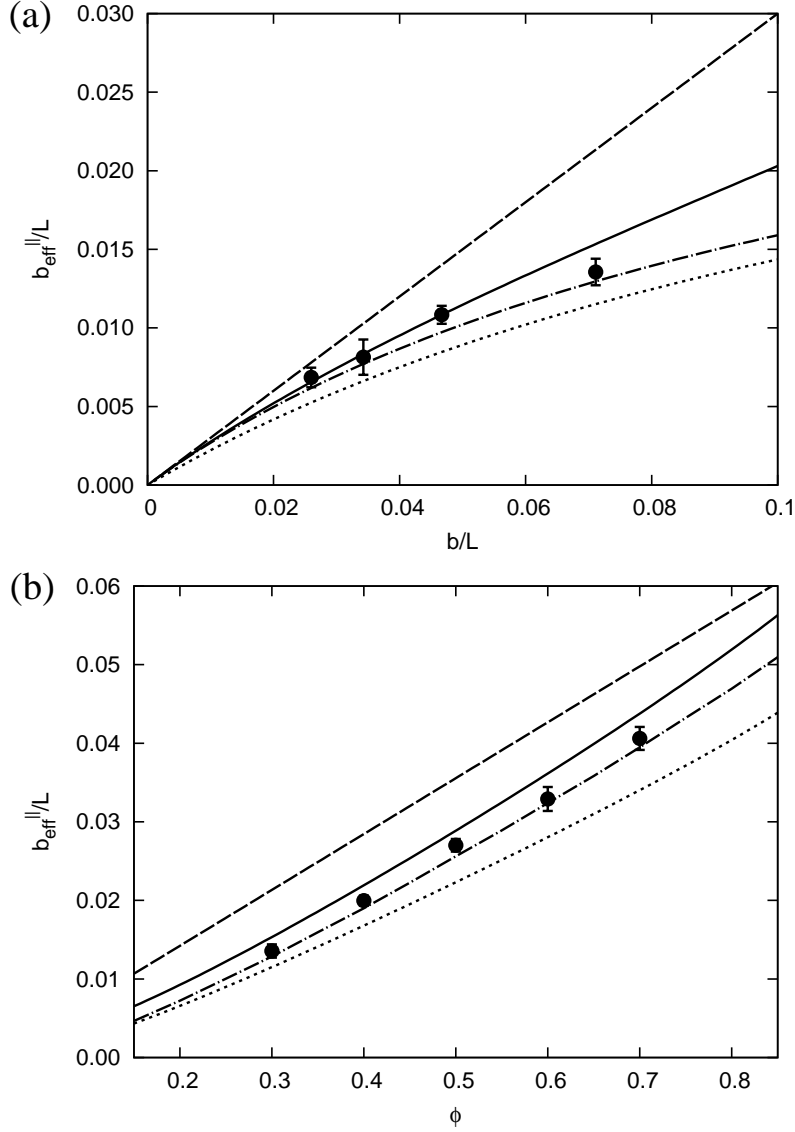


FIGURE 2. The longitudinal effective slip length as functions of (a) the local slip for the texture with $\phi = 0.3$, and (b) the fraction of the slipping phase at $b/L = 0.071$. Symbols are simulation data. Dash-dotted curves show exact numerical results, solid lines correspond to the two-term logarithmic expansions (Eq. (3.10)), dash lines to the linear theory (Eq. (1.1)), dotted lines to Eq. (5.1).

5. Results and Discussion

In this section, we compare predictions of our asymptotic theory with results of DPD simulations and direct numerical solutions of Eqs. (2.2)-(2.4) (see Appendix A for details of our numerical scheme).

Figures 2(a) and (b) show the exact numerical results and DPD simulation data for the longitudinal component of the slip-length tensor as a function of the dimensionless slip length b/L and the slipping area ϕ . The simulation data are in excellent agreement with the numerical results, confirming the validity of our DPD scheme. Similar calculations

were made for the transverse component of the slip-length tensor. All curves were found to be very similar to those presented in Figures 2, therefore, we do not show them here. The values for the transverse component are smaller than those for the longitudinal component, indicating that the flow is anisotropic. The simulation data in the transverse case tend to be slightly smaller than the prediction from the numerical solution. This has been observed previously Zhou *et al.* (2012) and can be related to the relatively large Reynolds numbers in our system (see Sec. 4). Inertia effect influence the flow past transverse stripes, as will be discussed below in the context of Figure 4. For flow past longitudinal stripes, the inertia effects are much smaller. Thus the DPD data shown in Fig. 2 are not affected by Reynolds number effects.

The surface-averaged slip, predicted by Eq. (1.1), is also shown in Figure 2 and is well above the exact values of the longitudinal effective slip. Also included in Figure 2 are the predictions of our theoretical result, Eq. (3.10). One can see that Eq. (3.10) indeed gives the correct asymptotic behavior in the limit of very small b/L . It slightly overestimates the value of the longitudinal effective slip at larger b/L . We remark and stress that nevertheless, our second-order calculation is much more accurate than Eq. (1.1).

Recently, Belyaev & Vinogradova (2010a) suggested approximate expressions for effective slip lengths of a surface decorated by partial slip stripes:

$$b_{\text{eff}}^{\parallel} \simeq \frac{L}{\pi} \frac{\ln \left[\sec \left(\frac{\pi\phi}{2} \right) \right]}{1 + \frac{L}{\pi b} \ln \left[\sec \left(\frac{\pi\phi}{2} \right) + \tan \left(\frac{\pi\phi}{2} \right) \right]}, \quad (5.1)$$

$$b_{\text{eff}}^{\perp} \simeq \frac{L}{2\pi} \frac{\ln \left[\sec \left(\frac{\pi\phi}{2} \right) \right]}{1 + \frac{L}{2\pi b} \ln \left[\sec \left(\frac{\pi\phi}{2} \right) + \tan \left(\frac{\pi\phi}{2} \right) \right]}. \quad (5.2)$$

These formulae have been verified (Belyaev & Vinogradova 2010a) using the method developed by Cottin-Bizonne *et al.* (2004). The agreement between the theoretical and numerical data was found to be very good for all ϕ and b/L , but at $b/L = O(1)$, small discrepancies were observed, suggesting that Eqs. (5.1) and (5.2) slightly underestimate the effective slip length. To examine this more closely, we also include the prediction of Eq. (5.1) in Figure 2. We find indeed a small discrepancy between the exact numerical data and the predictions of Eq. (5.1), which gives smaller values for the slip length. The same trends were observed in a wide range of ϕ , and the discrepancy slightly increases with the fraction of slipping phase. Still, the analytical expressions for the effective slip by Belyaev & Vinogradova (2010a) appear to be surprisingly accurate, given their simplicity. We stress, however, that they do not reproduce the asymptotic result, Eq. (1.1), in the limit of very small b/L . They do correctly predict a linear dependence on b in the limit of weakly slipping stripes

$$b_{\text{eff}}^{\parallel} = b_{\text{eff}}^{\perp} \simeq f(\phi) b, \quad (5.3)$$

but the prefactor, $f(\phi)$, differs from ϕ :

$$f(\phi) \simeq \frac{\ln \left[\sec \left(\frac{\pi\phi}{2} \right) \right]}{\ln \left[\sec \left(\frac{\pi\phi}{2} \right) + \tan \left(\frac{\pi\phi}{2} \right) \right]} < \phi \quad (5.4)$$

This prefactor corresponds to the slope of the curve $b_{\text{eff}}^{\parallel}(b)$ at $b/L = 0$. In Figure 2,

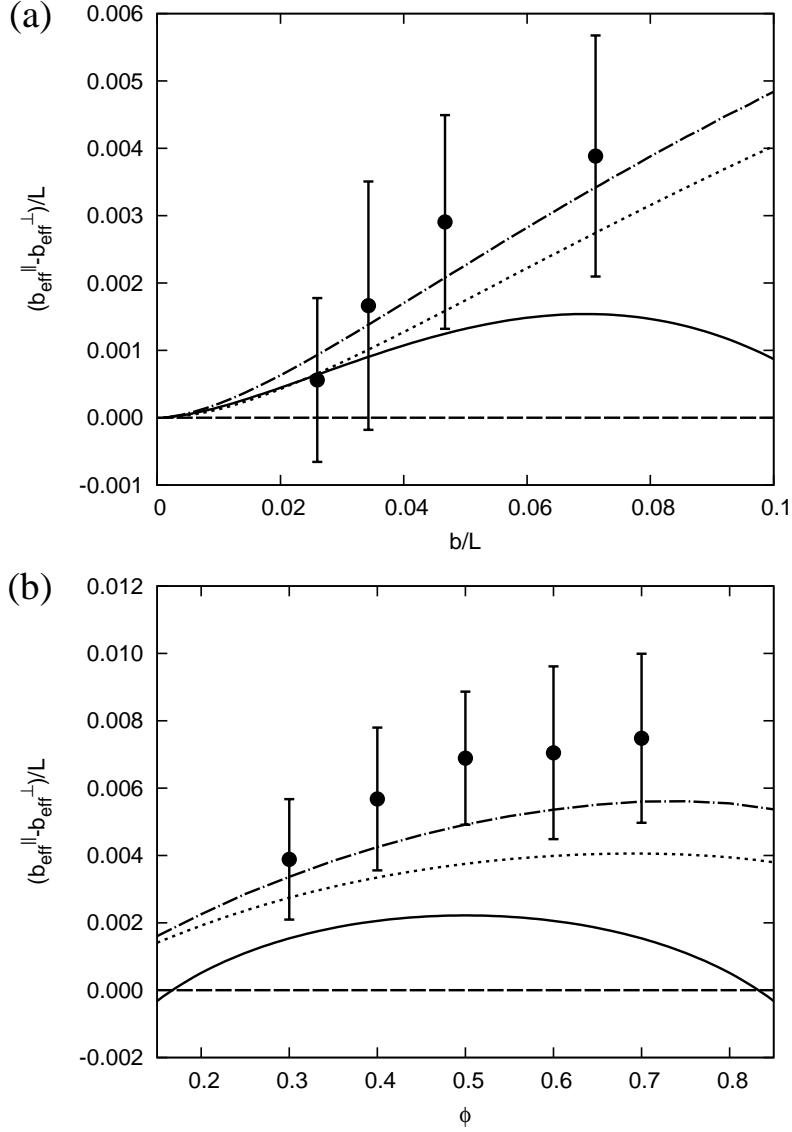


FIGURE 3. The difference between longitudinal and transverse effective slip lengths as functions of (a) the local slip for textures with $\phi = 0.3$, and (b) ϕ for textures with $b/L = 0.071$. Solid curves correspond to calculations made with the two-term logarithmic expansions [Eqs. (3.10) and (3.11)]. Dotted curves are obtained using Eqs. (5.1) and (5.2). Other notations are the same as in Figure 2.

the slope of the dotted line corresponding to Eq. (5.1) is smaller than the exact one. Nevertheless, the values of $b_{\text{eff}}^{\parallel}$ and b_{eff}^{\perp} given by (5.1) and (5.2) correlate well with the numerical data for all ϕ and small but finite b/L .

It has been predicted that in a thick channel the amplitude of a transverse flow, or the flow anisotropy, is controlled by the difference between the eigenvalues of the effective slip tensor, $b_{\text{eff}}^{\parallel} - b_{\text{eff}}^{\perp}$, which increases with ϕ and b (Vinogradova & Belyaev 2011). According to Eq.(1.1), this difference should vanish for weakly slipping surfaces. The effect of anisotropy is highlighted in Figure 3(a) and (b), which shows the difference

between the longitudinal and transverse effective slip lengths computed for fixed $\phi = 0.3$ and $b/L = 0.071$, respectively. The exact numerical values are positive, except in the case of extremely small local slip, clearly showing that the flow is anisotropic. This is confirmed by the simulation results. The error bars are relatively large. For weakly slipping surfaces, the difference $b_{\text{eff}}^{\parallel} - b_{\text{eff}}^{\perp}$ is small compared to the slip lengths themselves, (of the order of $\varepsilon^2 \ln \varepsilon$), and this is the reason for the large error of the simulation data. The simulation data agree with the numerical results within the error. Nevertheless, the data suggest that they lie systematically above the numerical results especially for larger slipping phase fraction ϕ . This is a consequence of the relatively large Reynold number. As discussed above, inertia effects primarily affect the flow and effective slip length in the transverse configuration. Test runs with larger shear rates were performed, and the deviations increased, indicating that they presumably vanish in the Stokes limit.

The results from the two-term logarithmic expansions, Eqs. (3.10) and (3.11), are also shown in Figure 3. In the limit of small b/L , the two-term expansion predicts correctly the positive difference and enhanced anisotropy as the slip length increases. At larger b/L , deviations from the numerical results become larger due to the increasing contribution from higher order terms. At $b/L = 0.071$, the two-term prediction for the slip length difference is only in moderately good agreement with the numerical data. For very low or very high coverage ($\phi \rightarrow 0$ or $\phi \rightarrow 1$), the agreement is not good at all, the theory even predicts the wrong sign [Figure 3(b)]. This is consistent with our discussion in Section 3.2, where we have argued that the approximation must break down when the singular regions associated with adjacent edges overlap. Also included in Figure 3 is the result from the approximate expressions Eqs. (5.1) and (5.2), which again shows surprisingly good agreement with the numerical data over the whole range of ϕ .

Figure 4(a) presents the longitudinal velocity at the wall for various b/L . In the simulations, the slip velocity has been obtained from an extrapolation procedure. Due to the small magnitude of the slip velocity in comparison to the thermal fluctuation (order of 1 for $k_B T = 1$), the data scatter very much. Much longer averaging times would be necessary to improve the statistics. The agreement of the exact numerical results and DPD simulation data is again very good. The velocity distribution is not smooth at the edge, instead it rises according to a power law on the slipping area with exponent close to $\lambda = 0.5$ as predicted in Section 3.2. In Figure 4(b), we verify the relation between the transverse and longitudinal velocities. Eq. (3.19) suggests that the local slip velocity above transverse stripes of slip length b should be identical to half of that above longitudinal stripes of slip length $2b$. This is confirmed by the numerical results. The simulation data, however, show deviations near the edge. This illustrates the origin of the finite Reynolds number effects discussed above. In simulations, the fluid is modelled as DPD particles with finite mass, and abrupt changes of the transverse velocity are suppressed because of inertia. Therefore the transverse velocity is smoothed out near the edge, showing a smaller value compared to the numerical data.

6. Concluding Remarks

In conclusion, we have investigated shear flow past weakly slipping super-hydrophobic stripes, focussing in particular on edge effects associated with steplike discontinuities in the local slip length. The essential conclusion from our analysis is that such step effects reduce the effective slip below the surface-averaged value and induce anisotropy. In practice, this means that the flow does not align with the applied shear stress. Thus, it should be possible to generate transverse hydrodynamic phenomena (like in Stone *et al.* (2004); Vinogradova & Belyaev (2011)) even with such weakly slipping anisotropic tex-

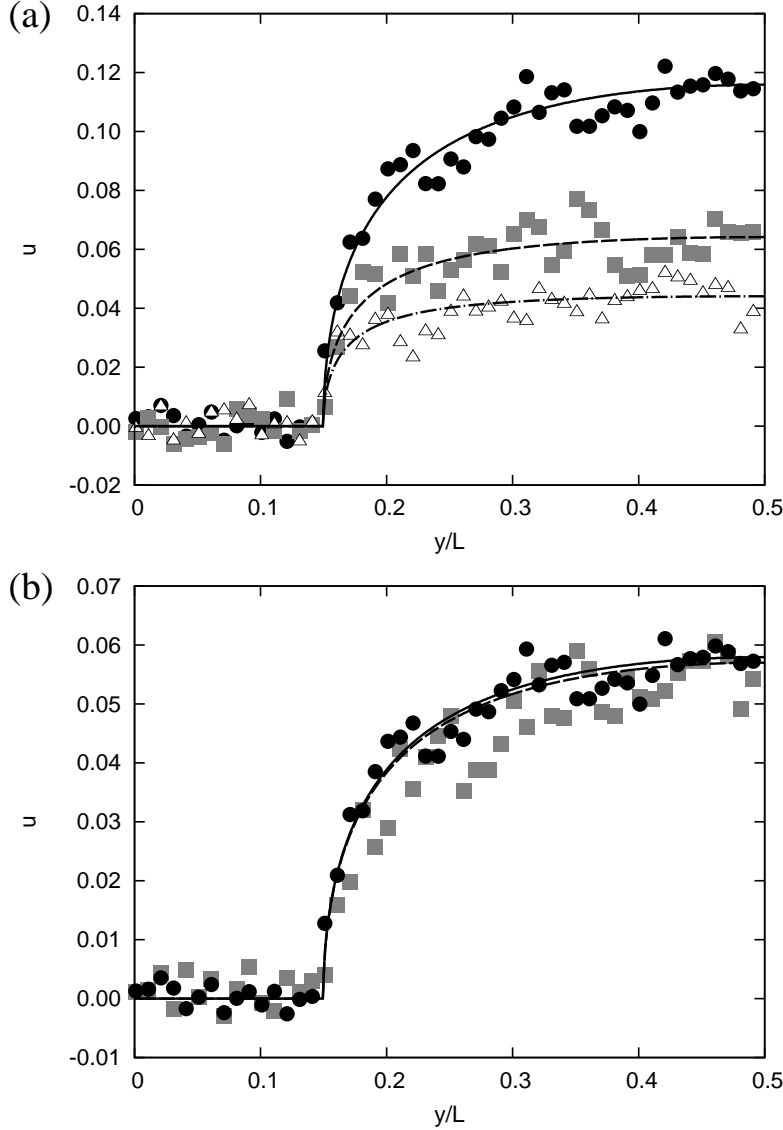


FIGURE 4. (a) The longitudinal velocity along the wall for a texture with $\phi = 0.7$ and different slip lengths: $b/L = 0.145$ (circles and solid line), $b/L = 0.071$ (squares and dashed line), and $b/L = 0.047$ (triangles and dash-dotted line). Symbols are simulation data and lines are numerical results. (b) Comparison of the transverse velocity ($v[y, z = 0, \beta(y)]$) and longitudinal velocity for nearly double local slip length ($\frac{1}{2}u_d[y, z = 0, 2\beta(y)]$, see Eq.(3.19)). The simulation and numerical results for longitudinal stripes of $b/L = 0.147$ are shown in circles and solid line, respectively. Squares and dashed line correspond to transverse stripes of $b/L = 0.071$.

tures. This may also have relevance for transverse electrokinetic phenomena (Bahga *et al.* 2010; Vinogradova & Belyaev 2011; Squires 2008; Belyaev & Vinogradova 2011). As a side remark, our analytical result opens the possibility of solving analytically many fundamental problems involving weakly slipping heterogeneous surfaces, including hydrodynamic interactions (Belyaev & Vinogradova 2010b; Asmolov *et al.* 2011).

Finally, we note, that even though our discussion has been limited to weakly slipping

heterogeneities, our model is much more general. Every result in this work could be used for describing weakly rough or porous surfaces since at large distances from the wall, the boundary condition at the rough interface or fluid-porous interface may be approximated by a slip model (Beavers & Joseph 1967; Taylor 1971; Richardson 1971; Kunert & Harting 2007; Kunert *et al.* 2010; Lecoq *et al.* 2004).

Appendix A. Numerical method

The Navier slip boundary condition (2.3) can be written in terms of the Fourier coefficients a^n , accounting for (3.1), as

$$\frac{a^0}{2} + \sum_{n=1}^{\infty} [1 + 2\pi n \varepsilon \beta(y)] a^n \cos(2\pi n y) = \varepsilon \beta(y). \quad (\text{A } 1)$$

To find a^n numerically we truncate the sum at some cut-off number N (usually $N = 512$) and apply a Fourier cosine transform to (A 1). The Fourier coefficients \tilde{A}_n^m and $\tilde{\beta}^m$ of the vectors $[1 + 2\pi n \varepsilon \beta(y_l)] \cos(2\pi n y_l)$ and $\beta(y_l)$, $y_l = l/2N$, $n, m, l = 0, \dots, N$, are evaluated using the IMSL routine FCOST. Then (A 1) is reduced to a linear system $\tilde{A}_n^m a^n = \tilde{\beta}^m$, which is solved using the routine LSARG. In view of (3.1), the application of FCOST to a vector $a^n \exp(-2\pi n z)$ produces an inverse Fourier transform, i.e., we evaluate $u(y_l, z)$ for given z .

Acknowledgments

This research was supported by the RAS through its priority program ‘Assembly and Investigation of Macromolecular Structures of New Generations’, and by the DFG through SFB-TR6. The simulations were carried out using computational resources at the John von Neumann Institute for Computing (NIC Jülich), the High Performance Computing Center Stuttgart (HLRS) and Mainz University (Mogon).

REFERENCES

- AJDARI, A. 2002 Transverse electrokinetic and microfluidic effects in micropatterned channels: Lubrication analysis for slab geometries. *Phys. Rev. E* **65** (1), 016301.
- ASMOLOV, E. S., BELYAEV, A. V. & VINOGRADOVA, O. I. 2011 Drag force on a sphere moving towards an anisotropic super-hydrophobic plane. *Phys. Rev. E* **84**, 026330.
- ASMOLOV, E. S. & VINOGRADOVA, O. I. 2012 Effective slip boundary conditions for arbitrary one-dimensional surfaces. *J. Fluid Mech.* **706**, 108–117.
- BAHGA, S. S., VINOGRADOVA, O. I. & BAZANT, M. Z. 2010 Anisotropic electro-osmotic flow over super-hydrophobic surfaces. *J. Fluid Mech.* **644**, 245–255.
- BAZANT, M. Z. & VINOGRADOVA, O. I. 2008 Tensorial hydrodynamic slip. *J. Fluid Mech.* **613**, 125–134.
- BEAVERS, G. & JOSEPH, D. 1967 Boundary conditions at a naturally permeable wall. *J. Fluid Mech.* **30**, 197–207.
- BELYAEV, A. V. & VINOGRADOVA, O. I. 2010a Effective slip in pressure-driven flow past super-hydrophobic stripes. *J. Fluid Mech.* **652**, 489–499.
- BELYAEV, A. V. & VINOGRADOVA, O. I. 2010b Hydrodynamic interaction with super-hydrophobic surfaces. *Soft Matter* **6**, 4563–4570.
- BELYAEV, A. V. & VINOGRADOVA, O. I. 2011 Electro-osmosis on anisotropic super-hydrophobic surfaces. *Phys. Rev. Lett.* **107**, 098301.
- BOCQUET, L. & BARRAT, J. L. 2007 Flow boundary conditions from nano- to micro- scales. *Soft Matter* **3**, 685–693.

- COTTIN-BIZONNE, C., BARENTIN, C., CHARLAIX, E., BOCQUET, L. & BARRAT, J. L. 2004 Dynamics of simple liquids at heterogeneous surfaces: Molecular-dynamics simulations and hydrodynamic description. *Eur. Phys. J. E* **15**, 427–438.
- ESPAÑOL, P. & WARREN, P. 1995 Statistical mechanics of dissipative particle dynamics. *Europhys. Lett.* **30**, 191.
- FEUILLEBOIS, F., BAZANT, M. Z. & VINOGRADOVA, O. I. 2009 Effective slip over superhydrophobic surfaces in thin channels. *Phys. Rev. Lett.* **102**, 026001.
- GAO, C. & GILCHRIST, J. F. 2008 Shear-induced particle migration in 1d, 2d, and 3d flows. *Phys. Rev. E* **78**, 025301.
- GROOT, R. D. & WARREN, P. B. 1997 Dissipative particle dynamics: bridging the gap between atomistic and mesoscopic simulation. *J. Chem. Phys.* **107**, 4423.
- KAMRIN, K., BAZANT, M. Z. & STONE, H. A. 2010 Effective slip boundary conditions for arbitrary periodic surfaces: the surface mobility tensor. *J. Fluid Mech.* **658**, 409–437.
- KOELMAN, J. M. V. A. & HOOGERBRUGGE, P. J. 1993 Dynamic simulations of hard-sphere suspensions under steady shear. *Europhys. Lett.* **21**, 363.
- KUNERT, C. & HARTING, J. 2007 Roughness induced boundary slip in microchannel flows. *Phys. Rev. Lett.* **99**, 176001.
- KUNERT, C., HARTING, J. & VINOGRADOVA, O. I. 2010 Random roughness hydrodynamic boundary conditions. *Phys. Rev. Lett.* **105**, 016001.
- LAUGA, E., BRENNER, M. P. & STONE, H. A. 2007 *Handbook of Experimental Fluid Dynamics*, chap. 19, pp. 1219–1240. NY: Springer.
- LECOQ, N., ANTHORE, R., CICHOCKI, B., SZYMCAK, P. & FEUILLEBOIS, F. 2004 *J. Fluid Mech.* **513**, 247–264.
- LIMBACH, H. J., ARNOLD, A., MANN, B. A. & HOLM, C. 2006 Espresso—an extensible simulation package for research on soft matter systems. *Comp. Phys. Comm.* **174**, 704.
- PRIEZJEV, N. V. 2011 Molecular diffusion and slip boundary conditions at smooth surfaces with periodic and random nanoscale textures. *J. Chem. Phys.* **135**, 204704.
- PRIEZJEV, N. V., DARHUBER, A. A. & TROIAN, S. M. 2005 Slip behavior in liquid films on surfaces of patterned wettability. *Phys. Rev. E* **71**, 041608.
- QUERE, D. 2008 Wetting and roughness. *Annu. Rev. Mater. Res.* **38**, 71–99.
- RICHARDSON, S. 1971 A model for the boundary condition of a porous material. Part 2. *J. Fluid Mech.* **49**, 327–336.
- SBRAGAGLIA, M. & PROSPERETTI, A. 2007 A note on the effective slip properties for microchannel flows with ultrahydrophobic surfaces. *Phys. Fluids* **19**, 043603.
- SCHMIESCHEK, S., BELYAEV, A. V., HARTING, J. & VINOGRADOVA, O. I. 2012 Tensorial slip of super-hydrophobic channels. *Phys. Rev. E* **85**, 016324.
- SMIATEK, J., ALLEN, M. & SCHMID, F. 2008 Tunable-slip boundaries for coarse-grained simulations of fluid flow. *Eur. Phys. J. E* **26**, 115–122.
- SODDEMANN, T., DÜNWEG, B. & KREMER, K. 2003 Dissipative particle dynamics: A useful thermostat for equilibrium and nonequilibrium molecular dynamics simulations. *Phys. Rev. E* **68**, 046702.
- SQUIRES, T. M. 2008 Electrokinetic flows over inhomogeneously slipping surfaces. *Phys. Fluids* **20**, 092105.
- SQUIRES, T. M. & QUAKE, S. R. 2005 Microfluidics: Fluid physics at the nanoliter scale. *Reviews of Modern Physics* **77**, 977.
- STONE, H. A., STROOCK, A. D. & AJDARI, A. 2004 Engineering flows in small devices. *Annual Review of Fluid Mechanics* **36**, 381–411.
- STROOCK, A. D., DERTINGER, S. K., WHITESIDES, G. M. & AJDARI, A. 2002a Patterning flows using grooved surfaces. *Anal. Chem.* **74**, 5306–5312.
- STROOCK, A. D., DERTINGER, S. K. W., AJDARI, A., MEZIĆ, I., STONE, H. A. & WHITESIDES, G. M. 2002b Chaotic Mixer for Microchannels. *Science* **295**, 647–651.
- TAYLOR, G. I. 1971 A model for the boundary condition of a porous material. Part 1. *J. Fluid Mech.* **49**, 319–326.
- VINOGRADOVA, O. I. 1999 Slippage of water over hydrophobic surfaces. *Int. J. Miner. Proc.* **56**, 31–60.
- VINOGRADOVA, O. I. & BELYAEV, A. V. 2011 Wetting, roughness and flow boundary conditions. *J. Phys.: Condens. Matter* **23**, 184104.

- VINOGRADOVA, O. I. & DUBOV, A. L. 2012 Superhydrophobic textures for microfluidics. *Mendeleev Commun.* **19**, 229–237.
- WANG, C. Y. 2003 Flow over a surface with parallel grooves. *Phys. Fluids* **15**, 1114–1121.
- YBERT, C., BARENTIN, C., COTTIN-BIZONNE, C., JOSEPH, P. & BOCQUET, L. 2007 Achieving large slip with superhydrophobic surfaces: Scaling laws for generic geometries. *Phys. Fluids* **19**, 123601.
- ZHOU, J. J., BELYAEV, A. V., SCHMID, F. & VINOGRADOVA, O. I. 2012 Anisotropic flow in striped superhydrophobic channels. *J. Chem. Phys.* **136**, 194706.